# 行政院國家科學委員會專題研究計畫 成果報告

## 拍翼式飛行器之研發與製作--子計畫二 : 拍翼式飛行器之飛行穩定控制與機電系統
## 研究成果報告(精簡版)

計 畫 類 別 ： 整合型
計 畫 編 號 ： NSC 97-2221-E-032-017-
執 行 期 間 ： 97 年 08 月 01 日至 98 年 07 月 31 日
執 行 單 位 ： 淡江大學航空太空工程學系

計 畫 主 持 人 ： 蕭富元
共 同 主 持 人 ： 洪健君
計畫參與人員 ： 碩士班研究生-兼任助理人員：楊澤明
碩士班研究生-兼任助理人員：陳正霖
碩士班研究生-兼任助理人員：蔣魁元
碩士班研究生-兼任助理人員：陳延銓
碩士班研究生-兼任助理人員：林鈺展
碩士班研究生-兼任助理人員：溫奕勛
碩士班研究生-兼任助理人員：林森煌

報 告 附 件 ： 出席國際會議研究心得報告及發表論文

處 理 方 式 ： 本計畫可公開查詢

中 華 民 國 98 年 10 月 30 日

# The Development of Flapping MAVs:
# The Stability Flight Control of a Flapping MAV and Its Avionics

蕭富元[1]、洪建君[2]
[1]淡江大學航空太空工程學系
[2]國防大學機電能源及航太工程學系

Abstract

The development of flapping MAVs, especially in the aspect of flight stability control and the avionics are studied in this research. The goal of this project is to investigate a possible control law and its implementation to stabilize the attitude of a flapping-wing robot, so that it can track navigation commands, achieve autonomous flight, and execute various missions. This work, as a subproject of "the Development of Flapping MAVs", was primarily lead by Dr. Fu-Yuen Hsiao, in charge of developing the control law to stabilize the flight of flapping MAVs, and collaborated with Dr. C.C. Hung, responsible for the development of Electro-mechanics system.

On the basis of the earlier knowledge on the Golden Snitch, a flapping-wing MAV in TKU, we stabilize the flight trajectory with a modified P-control. Different from other mechanical or aerial systems, the selections in control signal are limited in this problem due to the restrictions in carry-on weight. Numerical simulations also provided to demonstrate the robustness of our control law.

On the other hand, this research also presents the study of microstrip/meander-line antennas embedded into or deposited on flapping-MAV structures, and both the formulation and simulation of electromagnetic radiation characteristics of microstrip/meander-line antennas are introduced. The basic concepts of microstrip and meander-line antennas are introduced in the above analyses and some simulations of these antennas on 2D isotropic substrates are also demonstrated.

This report is essentially composed of two parts, the trajectory control and the development of micro avionics. Each part is detailedly presented in the format of paper by the investor. The ultimate goal of this research is to realize the autonomous flight of flapping-wing MAVs.

# The Flight Stability Control of a Flapping MAV

F.Y. Hsiao*

***Abstract*— The trajectory control of flapping-wing micro-aerial vehicles (MAVs) is discussed in this report. The Tamkang University (TKU) has been devoted to the development of flapping-wing robots for a long period, including design, fabrication and control. On the basis of the earlier knowledge on the Golden Snitch, a flapping-wing MAV in TKU, we stabilize the flight trajectory with a modified P-control. Different from other mechanical or aerial systems, the selections in control signal are limited in this problem due to the restrictions in carry-on weight. Numerical simulations also provided to demonstrate the robustness of our control law, and flight test will be scheduled to examine this design. The ultimate goal of this work is to realize the autonomous flight of flapping-wing MAVs.**
**Keyword: Micro Aerial Vehicles (MAVs), Flight dynamics, Trajectory control, P-Control**

## I. Introduction

This report studies the trajectory control of a flapping-wing MAV, especially the MAV developed in the Tamkang University. Flight in flapping is a very efficient way to transport a unit of mass over a unit of distance, even though it requires extremely high power output [8]. For this reason, it is an interesting field and a new generation technology for the researchers to investigate.

The TKU MEMS Laboratory has been developing bird-like flapping MAVs for several years, and the most recent prototype, "*Golden Snitch*", is a 8-gram-weight and 20-cm-wingspan aircraft including the fuselage, flapping wings, tail wing, battery, motor and a set of gear system. The flapping wing is driven by a motor with a four-bar linkage system. By adjusting the lengths of the four bars, various stroke angles can be designed. the stroke angle of *Golden Snitch* is designed around $53^\circ$. [4].

Researchers have been devoted themselves into the development of flapping-wing MAVs. Many theories about dynamics and control laws are come up with. Lighthill [7] performed some of the earliest theoretical studies on the aerodynamics of insect flight and Weis-Fogh and Jensen [11] determined the variation of the positional angle of fore and hind wings during flight of Schistocerca gregaria. A variety of experimental studies has enabled a better understanding of the nature of wing articulation by insects in hover and forward flight [3], [10], [12]. Moreover, several modeling and control laws are also proposed by researchers [1], [2], [5], [6], [9].

In this research, we investigate the trajectory control of flapping MAV. Although some researchers have been investigating this problems with application of various control theories, most of the results are not implementable in the current days. To implement those control law we requires powerful onboard computer and various sensors. However, these equipments are hardly possible to carry onboard, due to the limitation of size and weight. Consequently, we don't intend to propose a new or fascinating control law in this report. Instead, we focus on the practical problems about how to implement the control law and realize autonomous flight of the flapping MAV under current technology level.

In detail, taking the *Golden Snitch* as the example, we derive the equations of motion and obtain those dynamical coefficients with experimental data. To solve the weight problem, we select a commercial IR transmission module, which unfortunately constrains our control ability. We also propose an non-intrusive method, using stereo-vision, to obtain the position and attitude of the flapping-wing vehicle. Based on the current hardware that we can construct, a P-control with modified output feedback algorithm is proposed, and numerical simulations are provided to demonstrate the robustness of our algorithm.

## II. Dynamics Model

The flapping-wing MAV developed by the MEMS Laboratory in the Tamkang University, the *Golden Snitch*, is shown in 1, and its full nonlinear dynamics of this vehicle has been discussed in Ref. [14], provided the coordinate definition shown in Figs. 2 and 3.

In this report, however, we only consider the dynamics in the vertical motion with focus on the implementation of trajectory control law. Although realizing autonomous flight is the ultimate goal, in the current stage we are under the constraint of mechanisms, leading to the limited operation capability in flapping frequency and null ability in direction and attitude controls. As a consequence, this report mainly discuss the control law and implementation in vertical motion, and put the direction and attitude controls in future schedule.

Fig. 1. The *Golden Snitch* developed by the MEMS Lab in Tamkang University.

Fu-Yuen Hsiao is with faculty of Aerospace Engineering,Tamkang University, Tamsui 251, Taiwan, ROC fyhsiao@mail.tku.edu.tw

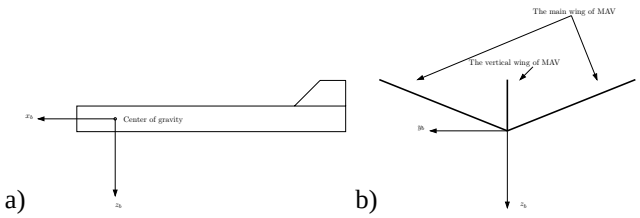


Fig. 2. A cartoon depicting the definition of the body-fixed frame.

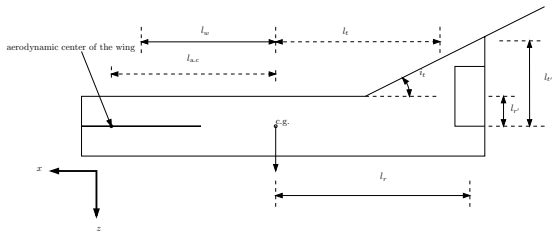


Fig. 3. A cartoon depicting the configuration parameters of the fuselage.

According to the Newton's second law, the dynamics of the vertical motion can be formulated as

$$\sum F_z \quad = \quad m\ddot{z}$$

where forces include the weight, $mg$, the averaged lift force over one flapping period generated by the main wing, $F_w$, and the lift force generated by the tail, $F_t$. Hence we expand the equation of motion as

$$F_w + F_t - mg \quad = \quad m\ddot{z} \tag{1}$$

According to Ref. [4] and [14], the lift forces of the main wing and the tail are functions of several parameters, given by

$$F_w \quad = \quad \frac{1}{2}\rho U^2 S_w C_{L_w} \tag{2}$$

$$F_t \quad = \quad \frac{1}{2}\rho U^2 S_t C_{L_t}, \tag{3}$$

respectively, where $\rho$ denotes the air density, $U$ the incoming wind speed, $S$ the area of the wing, and $C_L$ the lift coefficient. The subscript $w$ and $t$ denote the main wing and the tail, respectively. For simplicity, we would like to let $K_w = \rho S_w/2$ and $K_t = \rho S_t/2$, and replace those coefficients with $K_w$ and $K_t$ in future derivations.

The averaged lift coefficient over one flapping period generated by the main wing is a function of the advance ratio $J$ [14], given by

$$C_{L_w} \quad = \quad \zeta e^{-\eta J} + \xi \tag{4}$$

where the constants $\zeta$, $\eta$, and $\xi$ are functions of set angle. No theory so far is mature enough to predict those constants and the experimental values for the *Golden Snitch* are listed in Table I [4]. In addition, the advanced ratio, $J$, is defined as

$$J \quad = \quad \frac{U}{2bf\Phi} \tag{5}$$

where $\Phi$, $f$, and b are the stroke angle, flapping frequency, and semi-wingspan, respectively. The experimental values of the tail lift coefficient as a function of angle of attack are provided in Ref. [14] and listed in Table II.

TABLE I

THE CONSTANTS IN LIFT FORCE COEFFICIENT FOR *Golden Snitch*.

| Set angle | 10° | 20° | 30° | 40° | 50° |
|---|---|---|---|---|---|
| $\zeta$ | 19.07 | 20.22 | 35.35 | 42.09 | 58.25 |
| $\eta$ | 5.471 | 4.174 | 4.851 | 4.823 | 6.107 |
| $\xi$ | 0.6914 | 1.181 | 1.404 | 2.051 | 2.346 |

TABLE II

THE VALUES OF THE TAIL LIFT COEFFICIENT AS A FUNCTION OF AOA

| AOA | $-20°$ | $-10°$ | 0° | 10° |
|---|---|---|---|---|
| $C_{L_t}$ | -1.242 | -0.2808 | 0.3571 | 0.5963 |
| AOA | 20° | 30° | 40° | 50° |
| $C_{L_t}$ | 0.6881 | 0.8148 | 0.9025 | 0.8868 |

## III. HARDWARE

Aside from the dynamics of the *Golden Snitch*, we now turn to the hardware implemented for the control of the flapping-wing MAV. Different from a regular unmanned aerial vehicle, on which most control laws can be easily implemented, an MAV is greatly constrained by its size and weight. Consequently, implementation of control laws and realization of autonomous flight must take consideration of these two factors.

### A. Hardware Architecture

Figure 4 provides the traditional hardware architecture for the autonomous flight of unmanned aerial vehicles. Traditionally the aircraft is equipped with an onboard computer (OBC), in charge of communicating with ground station, receiving flight data from sensors/inertia measurement unit (IMU), and calculating control signals based on designed control law. Sensors or an IMU is also equipped onboard in order to collect flight data; antennas and encoder/decoder are also necessary for the purpose of communication. Trajectory is usually pre-assigned or controlled by the ground station via the communication module.

In the regime of MAV, however, the traditional architecture may not be suitable due to the limitation of size and weight. Take the *Golden Snitch* for example. We install a commercial

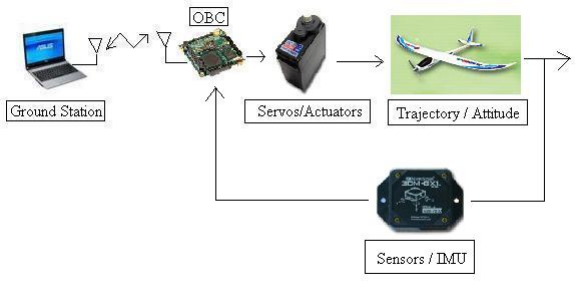


Fig. 4. The traditional hardware architecture for the autonomous flight of unmanned aerial vehicles.

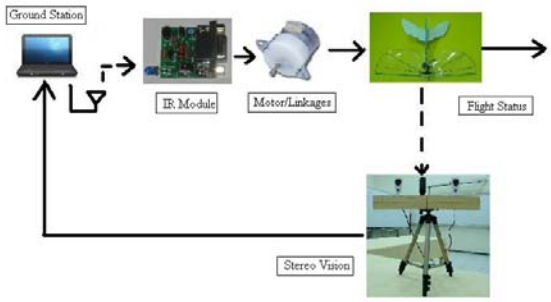


Fig. 5. The modified hardware architecture for the autonomous flight of our flapping-wing MAV.

infrared (IR) communication module (less than 1 grams) onboard, and keep the total weight of the vehicle under 10 gram. If the traditional architecture were to applied, the lightest RF communication module, including encoder and decoder, is ∼3 g, and the MEMS gyro is ∼30 g. These are definitely too heavy to apply, much less onboard computer or control chips.

A modified architecture is designed in this research, depicted in Fig. 5. As mentioned previously, the traditional RF communication module is replaced by a 1-gram IR module, and we developed an alternative navigation methodology using stereo vision. The guidance and control signal are accomplished and in the ground station, instead of onboard computer. As a result, we don't equip any onboard control unit in this research. This structure indeed confines the flight capability and applicability of the flapping-wing MAV, but it is the easiest and the only way to realize the autonomous flight nowadays.

### *B. The Communication Module of Golden Snitch*

As mentioned earlier the limitation of carry-on weight makes us select a specific commercial infrared communication module, which transmits signals in three channels, potentially applicable to control of the thrust, the direction, and the mode.

In channel one, 14 levels of signals are designated and applied to thrust control, corresponding to 14 spin rates of the driving motor, which drives the main wing through a four-bar linkage [4]. As a result, the 14 levels of signals generate thrusts through modifying the flapping frequencies. The relation between the thrust level and the flapping frequency is given in Table III. On the other hand, 6 levels of signals are are designated and reserved for future direction control. 3 levels of command can be assigned in each direction (right or left). Finally, one of three modes can be selected so that signals will not interfere with each other if more than one bird are flying.

Due to the constraint of the communication module, a regular state feedback or output feedback is not feasible since the control signal cannot be simply proportional to the state or output. A different control law must be investigated.

TABLE III

THE THRUST LEVEL AND THE FLAPPING RATE

| Thrust Level (No) | Flapping Rate (Hz) | Thrust Level (No) | Flapping Rate (Hz) | Thrust Level (No) | Flapping Rate (Hz) |
|---|---|---|---|---|---|
| 0 | 0 | 5 | 11.9 | 10 | 12.35 |
| 1 | 10 | 6 | 12.35 | 11 | 12.5 |
| 2 | 11.1 | 7 | 12.35 | 12 | 12.66 |
| 3 | 11.76 | 8 | 12.19 | 13 | 12.8 |
| 4 | 11.76 | 9 | 12.35 | 14 | 12.8 |

## IV. CONTROL LAW DESIGN

As stated previously this research mainly focuses on how the control law can be implemented in our robotic bird. Accordingly, a complicated control law is unrealistic since we only have limited choices in control signals. Therefore, the traditional P-control is investigated and shown robustness in practical implementation.

### *A. Linearized Dynamics*

The nonlinear dynamics describing the altitude of the vehicle is given in Eq. (1). Assume that the vehicle is original in the cruise condition: $z = z_0$, $\dot{z} = 0$, $U = U_0$, and $f = f_0$. Moreover, assume that the pitch angle of the fuselage is $\Theta$, as shown in Fig. 6(a). When in cruise condition, $\Theta = \Theta_0$. We conclude that the set angle for the main wing and angle of attack the tail are approximately $\alpha_w = \Theta_0 + c_w$ and $\alpha_t = \Theta_0 + c_t$, respectively. Here, $c_w$ and $c_t$ are certain constant, depending on the installation angle of the wings. Moreover, if the vehicle moves upward with a vertical speed

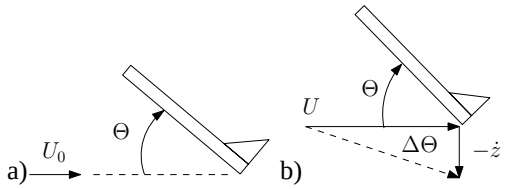


Fig. 6. A cartoon showing the incoming stream and fuselage pitch angle. a) The vehicle moves forward only; b) The vehicle also moves upward with speed $\dot{z}$.

$\dot{z}$, the angle of attack decreases by

$$\Delta\Theta \quad = \quad \tan^{-1}\frac{\dot{z}}{U} \tag{6}$$

as shown in Fig. 6(b).

To apply the P-control, we first linearize the dynamics about the cruise condition, given by

$$\delta F_w + \delta F_t \quad = \quad m\delta\ddot{z} \tag{7}$$

Consider the perturbation of the force generated by the main wing. Eqs. (2) and (4) indicate that the force is a function of $U$, $\zeta$, $\eta$, $\xi$, and $J$. Additionally, $J$ itself is a function of flapping frequency $f$, and $\{\zeta, \eta, \xi\}$ are functions of set angle $\Theta$. Therefore, we can write

$$F_w \quad = \quad F_w(U, \zeta, \eta, \xi, f)$$

The perturbation is then given by

$$\begin{aligned}\delta F_w \quad = \quad & \frac{\partial F_w}{\partial U}\delta U + \frac{\partial F_w}{\partial \zeta}\delta\zeta + \frac{\partial F_w}{\partial \eta}\delta\eta \\ & + \frac{\partial F_w}{\partial \xi}\delta\xi + \frac{\partial F_w}{\partial J}\delta J\end{aligned} \tag{8}$$

Assume the vehicle is suffered from vertical position and speed perturbations, $\delta z$ and $\delta \dot{z}$, respectively. Then we conclude

$$\begin{aligned}\delta U &= \frac{\partial U}{\partial \dot{z}}\delta \dot{z} \\ &= \frac{\partial}{\partial \dot{z}}\sqrt{U_0^2+\dot{z}^2}\Big|_{U=U_0,\dot{z}=0}\delta \dot{z} \\ &= 0 \end{aligned} \quad (9)$$

$$\delta\zeta = \frac{\partial \zeta}{\partial \Theta}\delta\Theta = \frac{\partial \zeta}{\partial \Theta}\frac{\partial \Theta}{\partial \dot{z}}\delta\dot{z} \quad (10)$$

$$\delta\eta = \frac{\partial \eta}{\partial \Theta}\delta\Theta = \frac{\partial \eta}{\partial \Theta}\frac{\partial \Theta}{\partial \dot{z}}\delta\dot{z} \quad (11)$$

$$\delta\xi = \frac{\partial \xi}{\partial \Theta}\delta\Theta = \frac{\partial \xi}{\partial \Theta}\frac{\partial \Theta}{\partial \dot{z}}\delta\dot{z} \quad (12)$$

As shown in Fig. 6(b), with an upward speed perturbation the influence to the fuselage angle of attack is given by

$$\frac{\partial \Theta}{\partial \dot{z}} = \Big(\tan^{-1}\frac{-\dot{z}}{U}\Big)\Big|_{U=U_0,\dot{z}=0} = -\frac{1}{U_0} \quad (13)$$

On the other hand, the perturbation of $J$ in terms of the change of control frequency $\delta f$ can be written as

$$\delta J = \frac{\partial J}{\partial f}\delta f = \frac{-U_0}{2b\Phi f_0^2}\delta f \quad (14)$$

As a result, the perturbation of $F_w$ can be expanded as

$$\begin{aligned}\delta F_w &= -\frac{1}{U_0}\Big(\frac{\partial F_w}{\partial \zeta}\frac{\partial \zeta}{\partial \Theta}+\frac{\partial F_w}{\partial \eta}\frac{\partial \eta}{\partial \Theta}+\frac{\partial F_w}{\partial \xi}\frac{\partial \xi}{\partial \Theta}\Big)\delta\dot{z} \\ &\quad +\frac{-U_0}{2b\Phi f_0^2}\frac{\partial F_w}{\partial J}\delta f \\ &= -K_wU_0\Big(e^{-\eta J}\frac{\partial \zeta}{\partial \Theta}-J\zeta e^{-\eta J}\frac{\partial \eta}{\partial \Theta}+\frac{\partial \xi}{\partial \Theta}\Big)\delta\dot{z} \\ &\quad +\frac{-U_0}{2b\Phi f_0^2}\frac{\partial F_w}{\partial J}\delta f \end{aligned} \quad (15)$$

Similarly, the perturbation of $F_t$ can be expanded as

$$\begin{aligned}\delta F_t &= \frac{\partial F_t}{\partial \Theta}\delta\Theta \\ &= K_tU_0^2\frac{\partial C_{L_t}}{\partial \Theta}\frac{\partial \Theta}{\partial \dot{z}}\dot{z} \\ &= -K_tU_0\frac{\partial C_{L_t}}{\partial \Theta}\delta\dot{z} \end{aligned} \quad (16)$$

For simplicity, we drop the sign "$\delta$" and denote the partial derivative of $(\cdot)$ with respect to $\Theta$ as $(\cdot)_{,\Theta}$ in the future derivation. The linearized equation of motion can then be written as

$$m\ddot{z}+B\dot{z} = Rf \quad (17)$$

where

$$\begin{aligned}B &= K_wU_0\Big(e^{-\eta J}\zeta_{,\Theta}-J\zeta e^{-\eta J}\eta_{,\Theta}+\xi_{,\Theta}\Big) \\ &\quad +K_tU_0C_{L_t,\Theta} \end{aligned} \quad (18)$$

$$R = K_wU_0^2\zeta\eta e^{-\eta J}\frac{U_0}{2b\Phi f_0^2} \quad (19)$$

### B. Control Law Design

The linearized equation of motion for the *Golden Snitch* is given in Eq. (17). As we can see, this is a very neat equation and can be controlled by using the traditional output feedback. The transfer function from the control adjustment to the vertical perturbation can be expressed as

$$\frac{z(s)}{f(s)} = \frac{R}{ms^2+Bs}$$

As a result, if a position feedback $f=-Kz$ is applied, this system will be stable anyway regardless of the value of $K$.

In our system, we have to consider the discontinuity of the control signal. As stated in the preceding sections, the nominal control is a set of 14 levels, denoting as $\{f_{0_1}, f_{0_2}, \cdots f_{0_{14}}\}$. Consider the cruise condition under input $f_{0_i}$. By taking the difference we obtain the sequence $f=\{\Delta f_k\}$, where $\Delta f_k = f_{0_i}-f_{0_k}$, $k=1,\cdots,14$.

As a result, if we consider the position feedback $f=-Kz$ with a pre-designed feedback gain $K$ and round it to the nearest element in the control sequence $\Delta f_k$, then we can view the system as a position feedback with gain $K'=\Delta f_k/z$. Since this system is stabilizable regardless of the value of the feedback gain, we conclude that this system will converge to the nominal state eventually.

## V. Numerical Simulations

The physical parameters of the *Golden Snitch* are provided in Table IV. The unit for length is *meter*; for mass is *gram*; for frequency is *Hz*; for angle is *rad*; and for the derivatives is *1/rad*. Based on those parameters we obtain $R=2.0541$ and $B=102.0409$. From the root locus analysis, the damping ratio is about 0.7 provided $K=300$.

TABLE IV
PHYSICAL PARAMETERS FOR *Golden Snitch*

| Item | Value | Item | Value | Item | Value |
|---|---|---|---|---|---|
| $m$ | 8 | $S_w$ | 0.014 | $S_t$ | 0.006 |
| $b$ | 0.2 | $\rho$ | 1230 | $U_0$ | 3.5 |
| $f_0$ | 12.66 | $\Theta$ | 0.3491 | $\Phi$ | 0.925 |
| $\zeta$ | 20.22 | $\eta$ | 4.174 | $\xi$ | 1.181 |
| $\zeta_{,\Theta}$ | 57.4276 | $\eta_{,\Theta}$ | 1.1007 | $\xi_{,\Theta}$ | 2.3945 |
| $C_{L,\Theta}$ | 2.1985 | | | | |

Figure 7 provides a simulation of this control law, rounding the feedback signal $f=-Kz$ to the nearest element in the control sequence $\Delta f_k$. At beginning we assume that the vehicle suffered from a vertical position offset by +10 cm. Then, as shown in Fig. 7 the control law starts to work and brings this vehicle back to the nominal height. Figure 8 demonstrates the control history. The solid line denotes the history by continuous control while the dashed line denotes the history by our current control module.

We can see that our current control module is less efficient because of the limitation in control capability. Therefore, originally they differ very much. Even so, the current control module, collaborated with the designated control law, still stabilizes the trajectory.

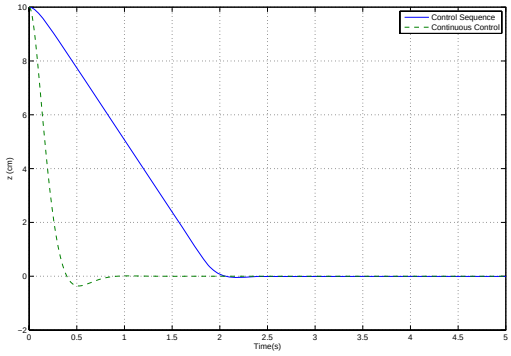


Fig. 7. Numerical simulation of trajectory. The Golden Snitch is assumed to be perturbed by 10 cm in height. Then the control law brings it back to the nominal successfully.

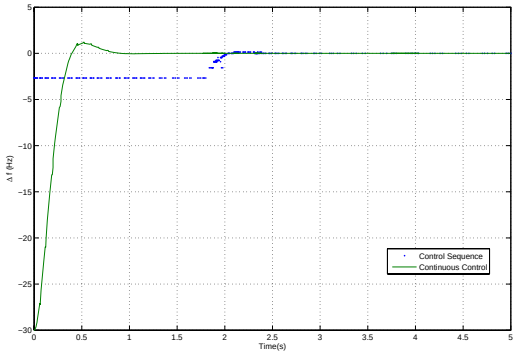


Fig. 8. Numerical simulation of control signal for the previous figure.

## VI. Conclusion

In this report we investigate a potential control law to stabilize our particular flapping-wing MAV developed in Tamkang University. At beginning we briefly review the required dynamics for the trajectory control. Wind tunnel experiments are also done to obtain physical and aerodynamical parameters and coefficients. We then introduce the hardware which is to be applied to the control of flight trajectory, especially focusing on the altitude control. Considering the capability limit of an MAV in carrying weight, we modify the control architecture so that automatic control of flight trajectory is possible using current technology, accomplished by a specific IR communication module and stereo vision. However, this modification also brings constraints to the usage of control law. Taking the constraint into account, we analytically prove that the traditional P-control with modified output feedback works very well in this case. Numerical simulations are also provided to demonstrate the robustness of our control law. Flight test will be the next step to examine this design after the hardware of the whole control loop is finished.

## VII. Acknowledgement

The authors wish to thank Dr. Lung-Jieh Yang and his research group for providing flight test and wind tunnel test data.

## References

[1] D. Campolo, L. Schenato, E. Guglielmelli, S.S. Sastry, "A LYAPUNOV-BASED APPROACH FOR THE CONTROL OF BIOMIMETIC ROBOTIC SYSTEMS WITH PERIODIC FORCING INPUTS", 2005 IFAC.

[2] X. Deng, L. Schenato, W.C. Wu , S.S. Sastry,"Flapping flight for biomimetic robotic insects: part I-system modeling,", *IEEE Transactions on Robotics*, Vol. 22, Iss. 4, Aug. 2006.

[3] C.P. Ellington, "The aerodynamics of hovering insect flight", *Philosophical Transactions of Royal Society of London*, B, 305, 1-181, 1984.

[4] C. K. Hsu, *The Preliminary Design, Fabrication, and Testing of Flapping Micro Aerial Vehicles*, Ph.D. Dissertation, Tamkang University, 2008

[5] Z.A. Khan, and S.K. Agrawal, "Control of Longitudinal Flight Dynamics of a Flapping-Wing Micro Air Vehicle Using Time-Averaged Model and Differential Flatness Based Controller," *Proceedings of the 2007 American Control Conference*, pp. 5284-5289, 2007

[6] Dae-Kwan Kim, and Jae-Hung Han, "Smart flapping wing using Macro-Fiber Composite actuators," Proceeding of Smart Structures and Materials, 2006

[7] Lighthill, *J. Mathematical Bio uidynamics*, Regional Conference Series in Applied Mathematics, SIAM, 1975.

[8] U.M. Norberg, *Vertebrate Flight: Mechanics, Physiology, Morphology, Ecology and Evolution*, Springer-Verlag, 1990

[9] L. Schenato, D. Campolo, and S. Sastry, "Controllability issuse in flapping flight for biomimic MAVs," *Proceedings of the 42nd IEEE Conference on Decision and Control*, pp. 6441-6447, 2003

[10] Z.J. Wang, J.M. Birch and M.H. Dickinson, "Unsteady forces and ow in low Reynolds number hovering flight: two dimensional computations vs. robotic wing experiments," *Journal of Experimental Biology*, 207, 449-460, 2004.

[11] T. Weis-Fogh, and M. Jensen, *Proceedings of the Royal Soceity B.* 239, pp. 415-584, 1956.

[12] A.P. Willmott, C.P. Ellington, and A.L.R. Thomas, "Flow visualization and unsteady aerodynamics in the ight of the hawkmoth", *Manduca sexta Philosophical Transactions of the Royal Society of London*, B, 352, 303-316, 1997.

[13] J. Yan, R.J. Wood, S.S. Avadhanula, and R.S.M. Fearing, "Towards flapping wing control for a micromechanical flying insect," *IEEE International Conference on Robotics and Automation*, 2001

[14] T.M. Yang and F.Y. Hsiao, "Dynamics of Flapping Micro-Aerial Vehicles", presented as Paper FrA07.6 at the *2009 American Control Conference*, St. Louis, MO, Jun. 10-12, 2009

# The development of Avionics for a Flapping MAV

洪健君

國防大學
機電能源及航太工程學系

**Abstract**

This research presents the study of microstrip/meander-line antennas embedded into or deposited on flapping-MAV structures, and both the formulation and simulation of electromagnetic radiation characteristics of microstrip/meander-line antennas are introduced. The basic concepts of microstrip and meander-line antennas are introduced in the above analyses and some simulations of these antennas on 2D isotropic substrates are also demonstrated.

**Keywords**: flapping MAV, microstrip antenna, meander-line antenna

## 1. Introduction

Conventional onboard dipole/monopole antennas mounted on aircraft fuselage often lead to disturbances in aerodynamic field. In high-performance aircraft, spacecraft, and missile applications, where size, weight, performance, installation, and aerodynamics are of major constraints, low profile antennas such as microstrip/meander-line antennas may be required. This research presents an innovative smart antenna module where the microstrip/meander-line antennas are embedded into or deposited on flapping-MAV (Micro-Unmanned Aerial Vehicle) structures for wireless communication.

The concept of microstrip antenna can be traced back to 1953 (Deschamps, 1953) and a patent in 1955 (Gutton and Baissinot, 1955). However, microstrip antennas have not received considerable attention until the 1970s due to the development of printed-circuit technology, the improved photolithographic techniques, the availability of good substrates with low loss tangent (a quantity related to substrate loss due to dielectric damping) and attractive mechanical properties. Microstrip antennas have matured considerably during the past 30 years, and many of the limitations have been overcome. Recently, numerical simulations using moment methods and finite difference techniques have available, and the interesting development of microstrip antennas has been the use of active device integrated directly in the antenna structure (Lin and Chuang, 1999).

The meander-line antennas were first proposed by Rashed and Tai (1982, 1991) for antenna size reduction by continuously folding the wire to reduce the resonant length. The meader-line antennas tend to resonate at frequencies much lower than a single element antenna of equal length, and an increase in the number of meander sections introduces less size reduction in return for an improved bandwidth. Moon (2001) adopted the folded meander-line structure and then covered the radiation element on the surface of multilayered dielectric chip. Michishita *et al*. (2004) reduced the size of meander line antenna by high permittivity material. Although the meander-line antennas can be simply fabricated by using modern printed-circuit technology and using the appropriate 2D electromagnetic analysis, the numerical simulation of antenna radiation characteristics will be necessary due to the radiation complexity of meander-line antenna on substrates.

## 2. Microstrip Antenna on Isotropic Substrates

The basic configuration of the microstrip antenna consists of a very thin metallic patch in a small fraction of one wavelength above the ground plane as shown in Fig.1. There are numerous isotropic substrates that can be used for microstrip antennas and their dielectric constants ($\varepsilon_r$) are usually in the range of $2.2 < \varepsilon_r < 12$. Thick substrates whose dielectric constant is in the lower end of the range are desirable because they provide better efficiency, higher bandwidth, loosely bound fields for radiation into space, but at the expense of larger element size (Pozar, 1987). The microstrip feed line is also a conducting strip, usually of much smaller width compared to the patch. The microstrip feed line is easy to fabricate, simple to match by controlling the insert position. However, such feeds are thus limited in bandwidth to about 2-5% for practical purposes (Pozar, 1992).

To overcome the difficulties of microstrip antennas embedded into or deposited on flapping MAVs, microstrip line feed will be adopted in this research because of its simplicity of fabrication and easy matching in the same plane of the patch located. For the rectangular patch and coordinate system shown in Fig.1, the lowest resonant frequency $(f_{rc})_{010}$ for the dominant $TM_{010}$ mode is given by (Bahl, 1982)

$$(f_{rc})_{010} = \frac{V_c}{2L_{eff}\sqrt{\varepsilon_{eff}}} = \frac{1}{2(L+2\Delta L)\sqrt{\varepsilon_{eff}}\sqrt{\mu_0\varepsilon_0}} = q\frac{V_c}{2L\sqrt{\varepsilon_r}}, \quad (1)$$

where

$$\Delta L = 0.412d \frac{(\varepsilon_{eff} + 0.3)\left(\frac{W}{d} + 0.264\right)}{(\varepsilon_{eff} - 0.258)\left(\frac{W}{d} + 0.8\right)}, \quad (2)$$

$$\varepsilon_{eff} = \frac{\varepsilon_r + 1}{2} + \frac{\varepsilon_r - 1}{2} \frac{1}{\sqrt{1 + 12d/W}} \quad \text{for } W/d > 1. \quad (3)$$

$V_c$ is the speed of light in free space, $\mu_0 = 4\pi \times 10^{-7} H/m$ is the permeability of free-space, $\varepsilon_0 = \frac{1}{36\pi} \times 10^{-9} F/m$ is the permittivity of free-space, $L$ is the physical length of the patch, $W$ is the width of the patch, $d$ is the thickness of the substrate, $L_{eff}$ is the effective length of the patch, $\Delta L$ is the extended incremental length due to fringing effects, $q$ is the fringe factor or length reduction factor, $\varepsilon_r$ and $\varepsilon_{eff}$ are the relative and effective dielectric constants, respectively.

Analytical description of a rectangular microstrip patch utilizes transmission-line theory to model the patch as two parallel radiating slots labeled as #1 and #2 as shown in Fig.1. The resonant input impedance $Z_{in}$ at the edge is then

$$Z_{in} = \frac{1}{2(G_1 \pm G_{12})} \approx \frac{1}{2G_1}, \quad (4)$$

where $G_1$ is the conductance of slot #1, and $G_{12}$ is the mutual conductance between slot #1 and #2,

$$G_1 = \frac{1}{120\pi^2} \int_0^{\pi} \left[ \frac{\sin(k_0 W/2 \cdot \cos\theta)}{\cos\theta} \right]^2 \sin^3\theta \, d\theta, \quad (5)$$

$$G_{12} = \frac{1}{120\pi} \int_0^{\pi} \left[ \frac{\sin(k_0 W/2 \cdot \cos\theta)}{\cos\theta} \right]^2 \cdot J_0(k_0 L \sin\theta) \sin^3\theta \, d\theta, \quad (6)$$

$k_0 = 2\pi/\lambda_0 = 2\pi f\sqrt{\mu_0 \varepsilon_0}$ is the wave number or propagation constant of free-space, $\lambda_0$ is the wavelength of free-space, $f$ is the operating frequency, $J_0$ is the Bessel function of the first kind of zero order. Typical values of the input impedance feeding at the edge are in the range of 150-300 ohms. The plus (+) sign in Eq.(4) is used for modes with odd or antisymmetric resonant voltage distribution beneath the patch and between the slots (e.g., the dominant $TM_{010}$ mode) while the minus (-) sign for modes with even or symmetric resonant voltage distribution.

Polarization of a radiated wave is defined as the property of an electromagnetic wave describing the time varying direction and relative magnitude of the electric-field vector. The polarization of an antenna in a given direction is defined as the polarization of the wave transmitted by the antenna. The sense of rotation for circular polarization (CP) is determined by observing the field rotation as the wave is viewed as it travels away from the observer. If the rotation is clockwise, the wave is right-hand circularly polarized (RHCP); if the rotation is counterclockwise, the wave is left-hand circularly polarized (LHCP). Circular polarization with only one feed can be achieved by a square patch with two truncated opposite corners as shown in Fig.2. The square patch is fed at the center of one of its side, and the antenna is fed along a center line as with a linear polarized patch. Right- or left-hand circular polarization depends on the location of the feed.

## 3. Design of Microstrip Antenna on 2D Isotropic Substrates

Analyses of square and rectangular patches on an isotropic substrate can be completed by using Eqs.(1-9). *Ansoft Ensemble*® is employed to simulate the microstrip patch on an isotropic substrate. Consider the microstrip patch on some FR4 substrate (e.g. $\varepsilon_r = 4.7$, $d = 1.6\,mm$) operating at 2.40 GHz, the geometry can be calculated as $L$ = 29.70 mm and $\Delta a$ = 2.42 mm. For a small section of 100-ohm feed line and a quarter-wave transformer attached to the corner-truncated CP patch, Fig.3(a) shows the dimension of this example, and the return loss is shown in Fig.3(b). The impedance bandwidth of 10dB is about 3% of the operating frequency. The return loss, i.e., the scatter parameter $S_{11}$ that describes the relation between incident and reflected power for microstrip patch, can be validated by treating the patch as a one-port element. The measurement of the return loss by network analyzer (e.g. Agilent EB362B) in Fig.3(b) is in good agreement with the simulation. Figure 3(c) is the far field pattern of electric field (*E*-field) operating at 2.40 GHz. The performance of RHCP feed is better than LHCP's because the maximum of LHCP *E*-field components is only about -10 dB of RHCP's. The patch is indeed suitable as an RHCP antenna.

## 4. Design of Meander-line Antenna on 2D Isotropic Substrates

Consider the prototype of meander-line antenna in Fig.4(a) on some isotropic FR4 substrate with finite ground plane ($21mm \times 2.5mm$) operating at 2.40 GHz, Fig.4(b) shows the simulation of return loss curve where the impedance bandwidth of 10dB is about 4.5% of the operating frequency. Figure 4(c) is the simulation of far field pattern of this example, the bold line is the *H*-plane diagram and the solid line is the *E*-plane diagram, respectively. This results show that the meander-line antenna in Fig.4(a) has the characteristic of omindirectional pattern in the upper and lower planes of the isotropic FR4 substrate. The far field pattern of *H*-field is less than that one of *E*-field due to the effect of instrinsic impedance. The measurements of the return loss by network analyzer (Anritsu 37347C) in Fig.4(d) and the far field pattern by anechoic chamber NSI 2000 in Fig.4(e) are in good agreement with the simulations of Figs.4(b) and 4(c), respectively. However, the design of meander-line antenna in Fig.4(a) does not give a good gain to meet the demands of wireless communication, so it is necessary to have a better design for flapping-MAV.

This research adopts better design for the

meander-line antenna with finite ground plane ($50mm \times 4.5mm$) as shown in Fig.5(a). Althrough the design of meander-line antenna of Fig.5(a) is only a bit different from that of Fig.4(a) in ground plane, gap and width, the value of antenna gain is higher than 6 dB over the design of meander-line antenna in Fig.4(a), i.e., over 4 times of that in the measurement of antenna gain. The return loss of design in Fig.5(a) is measured by network analyzer and shown in Fig.5(b), and the far field pattern are also measured and shown in Fig.5(c).

## 5. Conclusions

The basic concepts and designs of microstrip and meander-line antennas are introduced in the above analyses and some simulations of these antennas on 2D isotropic substrates are also demonstrated. The above analyses also show that the electromagnetic properties of microstrip/menader-line antennas on flapping-MAV structures could be evaluated by using the mentioned equations of the above analyses and an integral equation with a numerical technique, such as the MoM analysis in commercial software *Ansoft Ensemble*®. These designs of microstrip and meander-line antennas of this research will be recommended as basic configuration for the microstrip and meander-line antennas on flapping MAVs.

## 6. References


Bahl, I. J., Bhartia, P. and Stuchly, S. S., "Design of Microstrip Antennas Covered with a Dielectric Layer," *IEEE Trans. Antennas and Propagation*, vol. AP-30, no. 2, pp. 314-318, Mar 1982.

Deschamps, G. A., "Microstrip Microwave Antennas," presented at *the USAF Symposium on Antennas*, 1953.

Gutton, H. and Baissinot G., "Flat Aerial for Ultra High Frequency," *French Patent No. 703 113*, 1955.

Lin, S.-Y. and Chuang, H.-R., "Design of 2.4 GHz LNA/PA/Circularly-Polarized Active Microstrip Antennas," *Microwave Journal*, vol. 42, no. 1, pp. 22-37, Jan. 1999.

Michishita, N., Yamada, Y. and Nakakura, N., "Miniaturization of a Small Meander Line Antenna by Loading a High $\varepsilon_r$ Material," *The 5th International Symposium on Multi-Dimensional Mobile Communications Proceedings*, vol. 2, pp. 651-654, 2004.

Moon, S., "Folded Meander Line and Multilayered Dielectric Chip Antenna for Surface Mount," *Microwave Conference, Asia-Pacific*, vol. 2, pp. 472-475, Dec. 2001.

Pozar, D. M., "Radiation and Scattering from a Microstrip Patch on a Uniaxial Substrate," *IEEE Trans. Antennas and Propagation*, vol. AP-35, no. 6, pp. 613-621, Jun 1987.

Pozar, D. M., "Microstrip Antennas," *Proc. IEEE*, vol. 80, no. 1, pp. 79-81, Jan. 1992.

Rashed, J. and Tai, C. -T., "A New Class of Wire Antennas," *IEEE Antennas and Propagation Society International Symposium, AP-S Digest*, vol. 2, pp. 564-567, May 1982.

Rashed, J. and Tai, C. -T., "A New Class of Resonant Antennas," *IEEE Trans. Antenna and Propagation*, vol. 39, no. 9, pp. 1428-1430, Sep 1991.


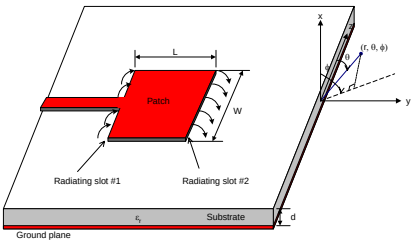


Figure 1 Rectangular microstrip antenna with microstrip line feed.

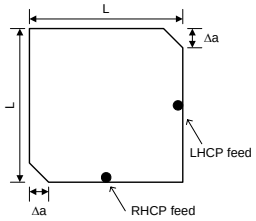


Figure 2 A corner-truncated circular polarized patch.

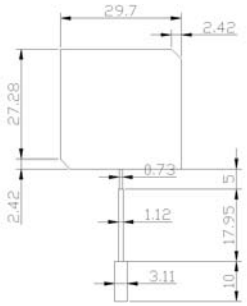


Figure 3(a) A corner-truncated circular polarized patch operating at 2.40 GHz.

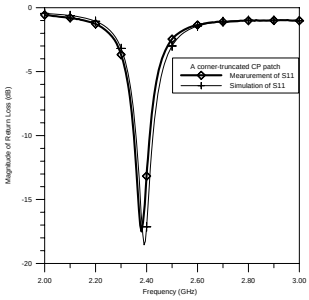


Figure 3(b) Simulation and measurement of the return loss (dB) of a corner-truncated patch operating at 2.40 GHz.

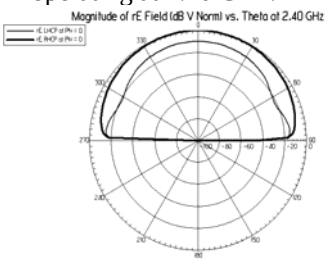


Figure 3(c) Far field for a corner-truncated patch operating at 2.40 GHz.

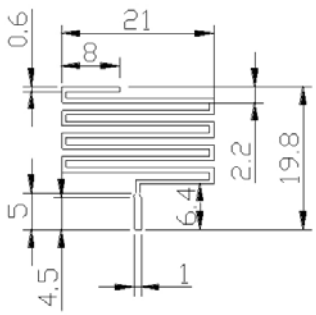


Figure 4(a) A meander-line antenna operating at 2.40 GHz.

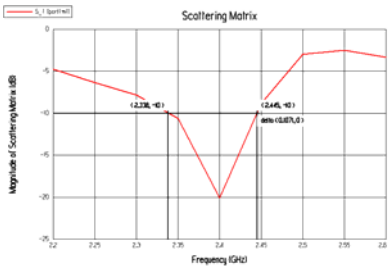


Figure 4(b) Simulation of the return loss of the meander-line antenna.

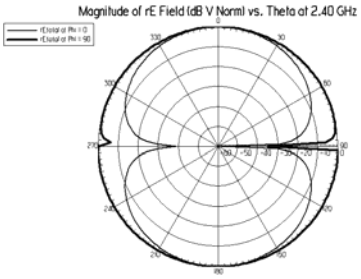


Figure 4(c) Simulation of the far field at 2.40 GHz of the meander-line antenna.

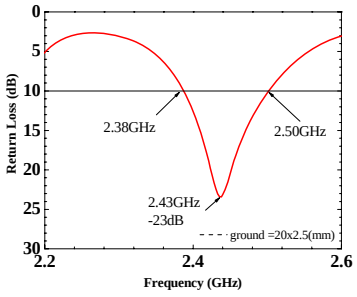


Figure 4(d) Measurement of the return loss of the meander-line antenna.

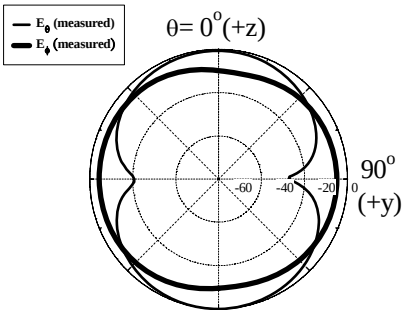


Figure 4(e) Measurement of the far field at 2.40 GHz of the meander-line antenna.

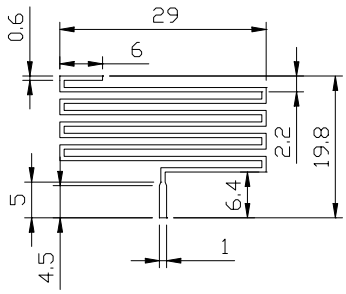


Figure 5(a) The better design of meander-line antenna operating at 2.40 GHz.

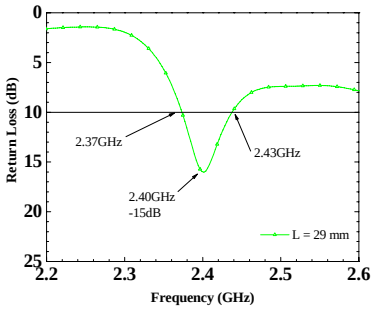


Figure 5(b) Measurement of the return loss of the better design of meander-line antenna.

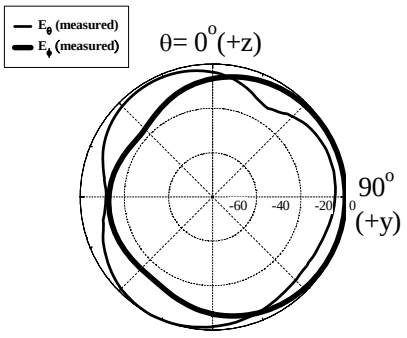


Figure 5(c) Measurement of the far field at 2.40 GHz of the better design of meander-line antenna.

# 行政院國家科學委員會補助國內專家學者出席國際學術會議報告

98 年 6 月 22 日

附件三

| | | | |
|---|---|---|---|
| 報告人姓名 | 蕭富元<br>Fu-Yuen Hsiao | 服務機構及職稱 | 淡江大學航太系<br>助理教授 |
| 時間<br>會議地點 | 98/6/10-98/6/12<br>St. Louis, MO, USA | 本會核定補助文號 | 國科會計劃編號:<br>97-2221-E-032-017- |
| 會議名稱 | (中文) 2009 年度美國控制學門年會<br>(英文) 2009 American Control Conference | | |
| 發表論文題目 | (中文) #FrA07.6 拍翼型微飛行器動力學分析<br>(英文) #FrA07.6 Dynamics of Flapping Micro-Aerial Vehicles | | |

報告內容應包括下列各項：

一、參加會議經過

6/ 9 抵達及註冊
6/10 與其它學者交流及討論
6/11 與其它學者交流及討論
6/12 上午發表論文 #FrA07.6
6/13 離開 St. Louis, MO

二、與會心得

American Control Conference 為美國控制學門之重要學術發表會。此次與會不僅有機會將本身之研究公之於世，亦是一個與全世界其它學者互相切磋之難得機會。在三天的會議之中，各界的學者不但對我的研究提出許多精闢的見解和意見，我也攜回了許多有用的資料，以做為日後研究時的參考。此外，我亦獲邀於明年度(2010) ACC 的”微飛行器特邀場次 (invited session)”發表最新研究，而且許多學者亦向我表示合作的興趣，為將來國際合作打開一扇窗。

三、考察參觀活動(無是項活動者省略)

無

四、建議

無

五、攜回資料名稱及內容

2009 American Control Conference Proceeding

六、其他

無

# Dynamics of Flapping Micro-Aerial Vehicles

T.M. Yang and F.Y. Hsiao

***Abstract*— The dynamics of flapping wing micro aerial vehicles (MAVs) is studied in this paper. The MEMS Laboratory in Tamkang University has been developing flapping-wing MAVs for several years. Based on the developed flapping-wing MAVs we study its dynamics and compare our results with flight test data. Although several papers have discussed similar topics previously, using our flight test data we demonstrate the validity of the assumptions and derivations. We also propose a claim that links the average aerodynamical forces to the wind tunnel test data, so that a flapping MAV can be analyzed with the same methodology as what we have done to a fixed-wing aircraft. Flight test data and numerical simulations are also provided to demonstrate the validity of our derivation.**

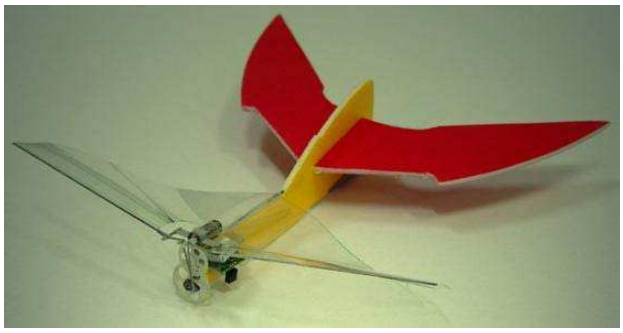

Fig. 1. The flapping MAV developed by the TKU MEMS Lab.[11]

## I. Introduction

Flight in flapping is a very efficient way to transport a unit of mass over a unit of distance, even thouth it requires extremely high power output[5]. For this reason, it is an interesting field and a new generation technology for the flight configuration. There are two kinds of flight configuration that is investigated in the literatures on natural flapping flight: Bird-like flight and Insect-like flight. The focus of this paper is on bird-like flight. The bird-like aerial robot we are investigating is developed by the TKU MEMS LAB in the recent years.

The TKU MEMS Laboratory has been developing bird-like flapping MAVs for several years. Figure 1 demonstrates the most recent prototype, "*Golden Snitch*", which is a 7-gram-weight and 20-cm-wingspan aircraft including the fuselage, flapping wings, tail wing, battery, motor and a set of gear system. The flapping wing is driven by a motor with a four-bar linkage system. By adjusting the lengths of the four bars, various stroke angles can be designed. In *Golden Snitch* the stroke angle is designed around $53°$. [2].

The aerodynamics performance in flapping animals consists of delayed stall, rotational circulation and wake capture [10]. These phenomenon and their functions can be explained by experiments and theories. However, complete and exact analysis of the flapping flight is not available because of the aerodynamic and mechanical complexity. As a result, In Ref. [4] Kim developed a smart flapping wing with a macro-fiber compositers (MFC) actuator to mimic the flying mechanism to measure the aerodynamic forces of flapping devices in wind tunnel test. Furthermore, In Ref. [7] Rakotomamonjy investigates the optimization of the flapping kinematics of the wing. In the full dynamic model of flapping MAV, Zaeem built a longitudinal flight dynamics with time-average theory [3], but only in 2-dimension space. In this paper, we intend to develop the three-dimensional model which will then be compared with the real trajectory.

In this research, we investigate the dynamic model of flapping MAV. Starting from Newton's second law we develop the equations of motion of our flapping-wing robot. Due to the fast flapping frequency compared with the translational and rotational rates, the average lift and thrust forces over each flapping period are applied to this model. Numerical simulations are also provided to examine the validity of our model and selected parameters.

## II. Dynamic Model

### A. Equations of Motion

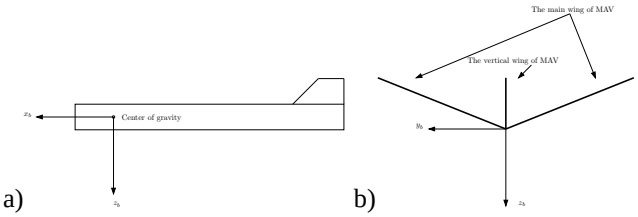


Fig. 2. A cartoon showing the definition of the body-fixed frame.

Before the formulation of equations of motion (EOM) a body-fixed frame is defined in Fig. 2. The $x_b$-axis points forward along the axis of the fuselage in the MAV's plane of symmetry. The $y_b$-axis is normal to the plane of symmetry pointing in the direction of the right wing. The $z_b$-axis then points downward in the MAV plane of symmetry, completing the right-handed Cartesian system. In addition, the coordinates in the inertial frame are denoted as $(x_f, y_f, z_f)$ in this paper. The transformation between these two frames can be

Tse-Ming Yang is with graduate student of Aerospace Engineering, Tamkang University, Tamsui 251, Taiwan, ROC 492370365@s92.tku.edu.tw

Fu-Yuen Hsiao is with faculty of Aerospace Engineering,Tamkang University, Tamsui 251, Taiwan, ROC fyhsiao@mail.tku.edu.tw

accomplished by a rotational matrix $\mathbf{R}$, satisfying

$$\mathbf{V}_f = \mathbf{R}\mathbf{V}_b \quad (1)$$

$$\dot{\mathbf{R}} = \mathbf{R}\tilde{\omega} \quad (2)$$

where $\mathbf{V}_f$ and $\mathbf{V}_b$ denote any vectors in the inertial and body-fixed frames, respectively. $\tilde{\omega}$ is the cross product operator of the angular velocity $\vec{\omega} = (\omega_x, \omega_y, \omega_z)$ [8].

The equations of motion of the flapping wing MAV can be obtained by applying Newton's second laws, given by

$$\sum \mathbf{F} = m\frac{d}{dt}\mathbf{V} + \omega \times (m\mathbf{V}) \quad (3)$$

$$\sum \mathbf{M} = \mathbf{I}\frac{d}{dt}\vec{\omega} + \vec{\omega} \times (\mathbf{I}\vec{\omega}) \quad (4)$$

where $\mathbf{I}$ denotes the inertia tensor. The external forces includes the weight of the vehicle, aerodynamical forces by flapping wing, horizontal tail wing, and vertical tail. Those forces also generates moments about the center of gravity (CG). We should notice that Eqs. (3) and (4) are the EOM described in the body-fixed frame, where the velocity in the body-fixed frame has components ($u$, $v$, $w$), and the angular velocity has components ($p$, $q$, $r$). The expansion of Eqs. (3) and (4) can be found in [6].

### *B. Averaging Theory and Formulation of Forces*

*1) Applicability of Averaging Theory:* Due to the periodic motion of the flapping wings, the averaging theory is usually applied to analyze the dynamics of a flapping wing robot, such as in Refs. [3] and [8]. The averaging theory is applicable based on the assumption that the wing is much lighter than the the body. As a result, the flapping wing slightly affects the vertical motion of the vehicle.

Even though the assumption sounds reasonable, it seems that no flight test data has been shown in the literature. In [3] a control law is designed based on this assumption while in [8] a *ground-based* experiment has been designed to investigate the controllability of a biomimic MAV.

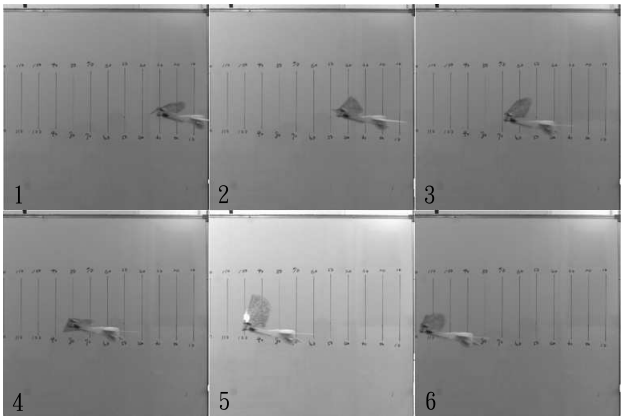


Fig. 3. The cruise flight of *Golden Snitch* catched by high speed CCD camera.[12]

Our *Golden Snitch*, however, verifies the validity of this assumption. As we can see in Fig. 3, *Golden Snitch* flies forward in a velocity of ∼3 m/s, but the fuselage still remains at an *almost* fixed height when the wings are flapping.

*2) Averaged Force and Advance Ratio:* In addition to the applicability of averaging theory, there was still one thing unclear before. Although the averaging theory was assumed to be applicable to the dynamical analysis of a flapping wing robot, the researchers in control field were still not clear about the formulation of the *averaged* lift and thrust forces. Accordingly, dynamics and control scientists usually simulated the lift and thrust force with a simple function, such as a periodic triangular wave.

On the other hand, the researchers in aerodynamics field always formulate the lift and thrust forces generated by a flapping wing as a function of the advance ratio, $J$, defined as

$$J = \frac{U}{2bf\Phi} \quad (5)$$

where $\Phi$, $f$, and b are stroke angle, flapping frequency, and wing semi-span, respectively. Typically, unsteady-state flight has advance ratio $J$ less than 1. Low advance ratio $J$ is an indication that these flyers must flap their wings at high speed compared to the speed of their flights in order to stay aloft. Therefore, the regime of $J < 1$ is dominated by unsteady-state flight. On the other hand, for $J \gg 1$, the flight regime becomes quasi-steady and approaches steady-state. For example, a fixed-wing airplane operates in the regime of $J$ near infinite because the wings' flapping frequency is zero. The lift and thrust forces can be expressed as functions of $J$ [2]

$$F_{\text{lift}} = \frac{1}{2}\rho U^2 S C_L(J) \quad (6)$$

$$F_{\text{thrust}} = \frac{1}{2}\rho U^2 S C_T(J) \quad (7)$$

where $C_L(J)$ and $C_T(J)$, as functions of $J$, denote the lift coefficient and thrust coefficient, respectively.

Here we claim that *the forces calculated from the lift or thrust coefficient as a function of $J$ can be treated as the averaged force*. A simple proof goes below. Consider

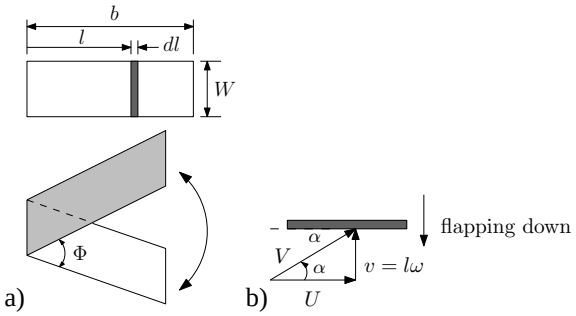


Fig. 4. A cartoon showing the definition of wing parameters.

a very thing rectangular wing, as shown in Fig. 4(a), with length $b$, width $W$, stroke angle $\Phi$, and flapping frequency $\omega = 2\pi f$. Assume the setting angle is zero so that the angle of attack (AOA) is determined by the attacking angle of the incoming air stream completely. Consider a small area element on the wing, whose flapping motion is shown in

Fig. 4(b). According to aerodynamics theory, the lift force generated by this element is formulated as

$$dF = \frac{1}{2}\rho V^2 C_L(\alpha) dA \quad (8)$$

where $V^2 = U^2 + (l\omega)^2$, $dA = W dl$, and

$$\alpha = \arctan\left(\frac{l\omega}{U}\right)$$

To simplify the notation we define $l/b = \gamma$. Introducing the advance ratio we obtain

$$l\omega = \frac{\gamma\pi}{J\Phi} U$$

As a result, Eq. (8) can be reformulated as

$$\begin{aligned} dF &= \frac{1}{2}\rho V^2 C_L(\alpha) dS \\ &= \frac{1}{2}\rho U^2 W b \left[1 + \left(\frac{\pi}{J\Phi}\right)^2 \gamma^2\right] C_L(\alpha) d\gamma \\ &= \frac{1}{2}\rho U^2 S \left[1 + \left(\frac{\pi}{J\Phi}\right)^2 \gamma^2\right] C_L(\alpha) d\gamma \end{aligned} \quad (9)$$

where $S = Wb$ is the total area of the wing, and $\alpha = \alpha(J, \gamma)$. Consider the average force during the downstroke during time interval $T_d$, given by

$$\begin{aligned} \bar{F} &= \frac{1}{T_d}\int_0^{T_d} F(t) dt \\ &= \frac{1}{T_d}\int_0^{T_d}\int_0^{F} dF\, dt \\ &= \frac{\rho U^2 S}{2T_d}\int_0^{T_d}\int_0^{1} \left[1 + \left(\frac{\pi}{J\Phi}\right)^2 \gamma^2\right] C_L(\alpha) d\gamma\, dt \end{aligned}$$

Since the integrant is not an explicit function of time, we can integrate with respect of time first and null out $T_d$. Therefore,

$$\bar{F} = \frac{\rho U^2 S}{2}\int_0^1 \left[1 + \left(\frac{\pi}{J\Phi}\right)^2 \gamma^2\right] C_L(\alpha(J,\gamma)) d\gamma$$

Define

$$C'_L(J) = \int_0^1 \left[1 + \left(\frac{\pi}{J\Phi}\right)^2 \gamma^2\right] C_L(\alpha(J,\gamma)) d\gamma$$

We obtain that

$$\bar{F}_d = \frac{1}{2}\rho U^2 S C'_{L_d}(J) \quad (10)$$

where the subscript $d$ denotes *downstroke*. Similarly, the average force during the upstroke is given by

$$\bar{F}_u = \frac{1}{2}\rho U^2 S C'_{L_u}(J) \quad (11)$$

As a result, the average force generated during a complete flapping is given by

$$\begin{aligned} \bar{F} &= \bar{F}_d + \bar{F}_u \\ &= \frac{1}{2}\rho U^2 S C'_{L_d}(J) + \frac{1}{2}\rho U^2 S C'_{L_u}(J) \\ &= \frac{1}{2}\rho U^2 S C'_L(J) \end{aligned} \quad (12)$$

where $C'_L(J) = C'_{L_d}(J) + C'_{L_u}(J)$. We can see that the average force has the same formulation as Eqs. (6) and (7).

We would admit that this is not a rigorous proof because many aerodynamics factors are not considered, such as the stability of the air flow, the flexibility of the wing and so on. However, at least this proof gives a qualitative link between the average force used in the dynamics field and the most common way to formulate flapping lift and trust forces in the aerodynamics field. In other words, if we have the lift and thrust coefficient curves at hand, which are usually easy to obtain in aerodynamics journals, we can simply apply the same methodology of analyzing a fixed-wing vehicle to the analysis of a flapping-wing robot.

### C. Formulation of Forces and Moments

Having shown that the average forces over one flapping period can be calculated by using Eqs. (6) and (7), which is independent of time, we conclude that the methodology to analyze a fixed wing vehicle can be applied to the flapping wing vehicle. There are only two differences. First of all, the force coefficients $C_L$ and $C_T$ are no longer functions of angle of attack only, but also functions of advance ratio. Second, when applied to analyze the dynamics of the whole vehicle, we don't use angle of attack since it is not rigorously defined in flapping motion. Instead, the set angle and stroke angle are introduced.

Figures. 5(a) and (b) provide the distribution of aerodynamics forces on the wing. As a result, provided Eqs. (6) and (7) $F_{x_b}$ and $F_{z_b}$ can be obtained by considering the vector addition of the lift and thrust forces.

$$F_{z_{b_{wing}}} = F_{thrust}\sin(\alpha) - F_{lift}\cos(\alpha) \quad (13)$$

$$F_{x_{b_{wing}}} = F_{thrust}\cos(\alpha) + F_{lift}\sin(\alpha) \quad (14)$$

where $\alpha$ is set angle of MAV.

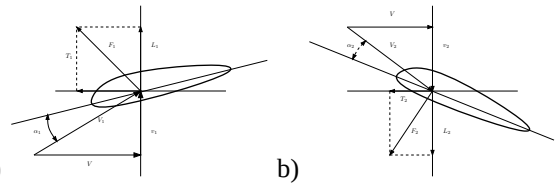

a) b)

Fig. 5. The aerodynamic force distribution during a)downstroke. b) upstroke.

On the other hand, the moments exerted on the MAV can be obtained through summing up all individual moment and torque. All the necessary geometric parameters to calculate moments are shown in Fig. 6. In addition to the regular formulation of moments, one thing to remind again is that we have to consider the torque applied by the motor, $\tau = \tau_{\text{motor}}$ pointing along $+x_b$-axis because our motor spins clockwise. Applying the formulated forces and moments to Eqs. (3)-(4) we can solve for the position, velocity and attitude of the MAV.

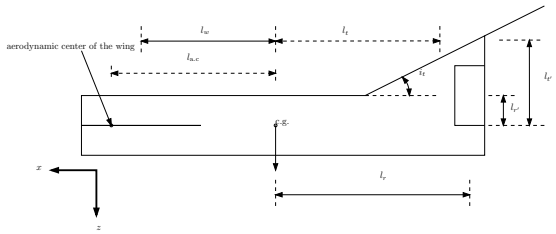


Fig. 6. A cartoon showing the geometric parameters of the fuselage.

| Set angle | 10° | 20° | 30° | 40° | 50° |
|---|---|---|---|---|---|
| $a$ | 19.07 | 20.22 | 35.35 | 42.09 | 58.25 |
| $b$ | 5.471 | 4.174 | 4.851 | 4.823 | 6.107 |
| $c$ | 0.6914 | 1.181 | 1.404 | 2.051 | 2.346 |
| $a'$ | 109.8 | 103.9 | 153.2 | 156.2 | 92.43 |
| $b'$ | 7.878 | 8.168 | 11.05 | 10.58 | 9.154 |
| $c'$ | 0.3139 | 0.1475 | 0.01054 | -0.5002 | -0.8389 |

TABLE I

THE PARAMETERS IN FORCE COEFFICIENTS FOR A FLAPPING WING.[2]

### D. Coefficients of the Main Wing

According to Ref. [1], the coefficient of lift and coefficient of thrust can be modeled as:

$$C_{L_{wing}} = ae^{-bJ} + c \tag{15}$$

$$C_{T_{wing}} = a'e^{-b'J} + c' \tag{16}$$

For the TKU flapping MAV, those parameters are obtained through wind tunnel test, and list as a function of set angle in Tab. (I). With the lift and thrust coefficients, the forces can be obtained using Eqs. (6) and (7). According to the result from the proceeding section, the obtained forces will be the average ones over one flapping period. An example showing the variation of forces as a function of time is shown in Figs. 7 and 8.

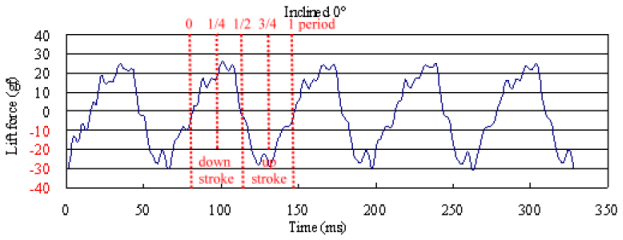


Fig. 7. The variation of lift force during a flapping period.[2]

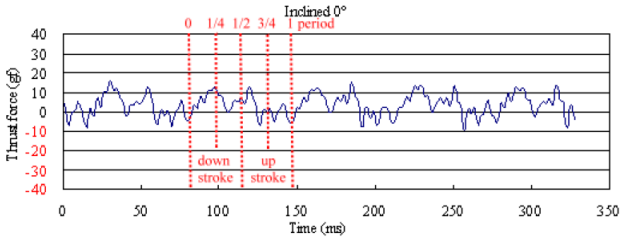


Fig. 8. The variation of thrust force during a flapping period.[2]

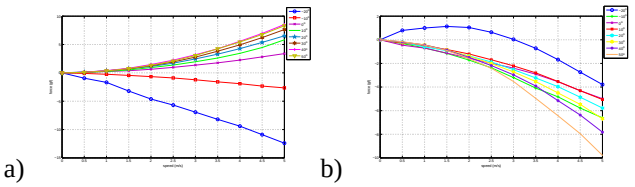


Fig. 9. The lift and drag performance of tail wing in wind tunnel test.

| AOA | $-20^o$ | $-10^o$ | $0^o$ | $10^o$ | $20^o$ | $30^o$ | $40^o$ | $50^o$ |
|---|---|---|---|---|---|---|---|---|
| $C_{L_{tail}}$ | -1.242 | -0.2808 | 0.3571 | 0.5963 | 0.6881 | 0.8148 | 0.9025 | 0.8868 |
| $C_{D_{tail}}$ | -0.4868 | -0.695 | -0.4938 | -0.5229 | -0.5974 | -0.6971 | -0.8186 | -1.04 |

TABLE II

THE PARAMETERS IN FORCE COEFFICIENTS FOR A TAIL WING.

### E. Coefficients of the Horizontal Wing

In addition to the main wing, the tail wing is still to be considered. The tail-wing parameters of aerodynamic forces is obtained through wind tunnel test, shown in Figs. 9(a) and (b). The tail-wing angle of attack ranges from $-20^o$ to $50^o$ and wind speed ranges from $0$ m/s to $5$ m/s.

According to aerodynamics, lift and drag coefficients are given by

$$C_{L_{tail}} = \frac{2L_{tail}}{\rho U^2 S_{tail}} \tag{17}$$

$$C_{D_{tail}} = \frac{2D_{tail}}{\rho U^2 S_{tail}} \tag{18}$$

$$\tag{19}$$

where $\rho$ is density of air, $S_{tail}$ is the area of the tail wing, $L_{tail}$ and $D_{tail}$ denote the lift and drag of the tail wing, respectively. For *Golden Snitch*, the area of tail wing is about $6013.715\ \mathrm{mm}^2$, and the density of air is about $1.23\ \mathrm{kg/m}^3$. Hence,

$$C_{L_{tail}}U^2 = 2.65L_{tail} \tag{20}$$

$$C_{D_{tail}}U^2 = 2.65D_{tail} \tag{21}$$

where the unit of $U$ and $L_{tail}(D_{tail})$ are $\mathrm{m/s}$ and $\mathrm{gf}$, respectively.

## III. Flight Test and Numerical Simulation

Having shown that the averaging theory is applicable to the flapping wing MAV, and the way to obtain the average forces from experiment data, we apply this result to the analysis of our *Golden Snitch*.

### A. Flight Test

The *Golden Snitch* has been put into flight test and its flight duration is about 5 minutes. Some examples of the flight trajectory are provided in Figs. 10- 12 [2]. The only control applied to this vehicle is the spin rate of the motor, which controls the flapping frequency. Currently, there is no control of direction. The flight trajectory, however, is spiral. This is resulted from the torque generated by the motor due to the conservation of angular momentum.

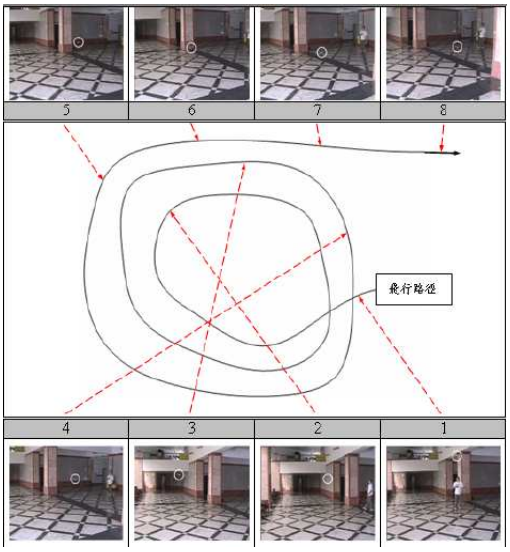


Fig. 10. An example of the flight test trajectory. [2]

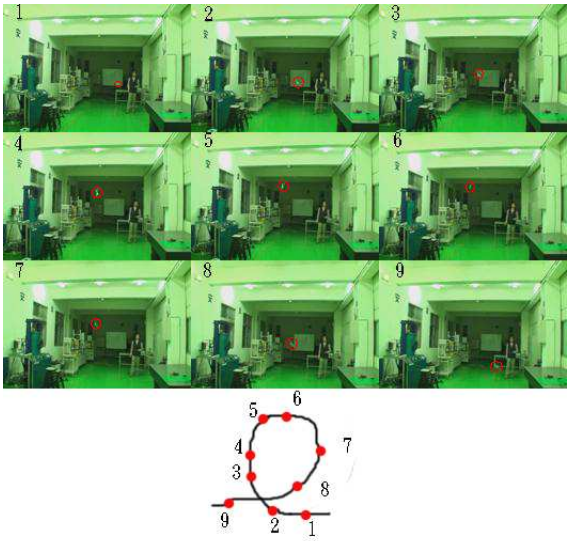


Fig. 11. An example of the flight test trajectory. [2]

## B. Numerical Simulation

*1) Attitude Equilibria at Cruise Flight:* At cruise flight the MAV must be in the equilibria of its attitude. According to our model, we obtain that the pitch angle at cruise flight must be $12°$. Examining Fig. 3 we realize that the *Golden Snitch* flies at the angle of $15°$. This is encouraging since our prediction is quite close to the reality. However, this fact also implies that the predicted lift force at wing tail may be too large so that the pitch angle is smaller than the real one.

*2) Simulated Flight Trajectories:* Besides encouraging result in the match of derived and actual attitude equilibria, three dynamical cases are also simulated, provided in Figs. 13- 15. In the first case, shown in Fig. 13, we use the derived parameters from the previous chapter but neglect the torque made by the motor. The simulated flight trajectory forms a circle. In the second case we reduce the coefficients

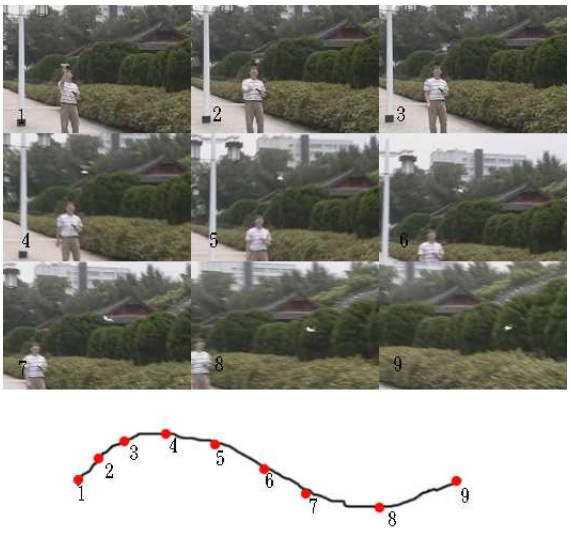


Fig. 12. An example of the flight test trajectory. [2]

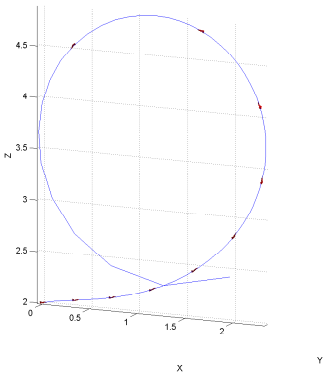


Fig. 13. The flight trajectory in case 1.

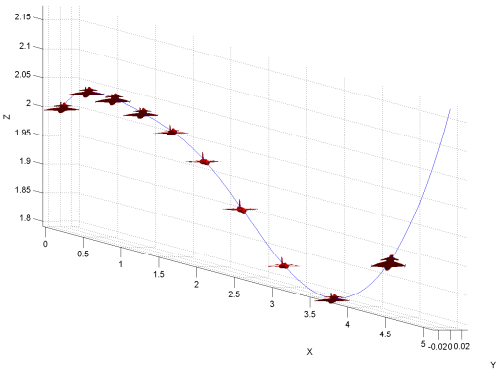


Fig. 14. The flight trajectory in case 2.

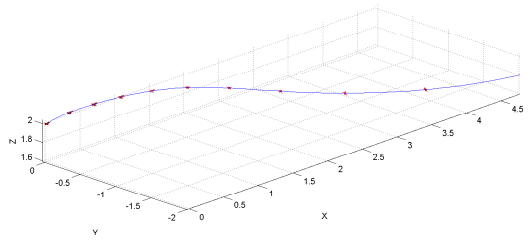


Fig. 15. The flight trajectory in case 3.

of main wing by half. The flight trajectory is presented in Fig. 14. In the case 3, we take into consideration the torque generated by the motor and use treat other parameters the same as in case 2. The flight trajectory is shown in Fig. 15.

*3) Discussion:* In the simulation of case 1, the moment in $y_b$ direction seems too large and that makes MAVs do a circular motion. This simulation matches one case in flight test, given in Fig. 11. In the case 2 we reduce half of the lift and thrust coefficients. This time the MAV stays reasonable flight for longer time, but it still attempts to do a circular motion, too. It is obvious that this simulation resembles the case shown in Fig. 12. A reasonable explanation goes that the lift might be smaller outdoors since there exist disturbances. As a result, the simulation assumption in case 2 is also reasonable. In case 3, we consider the torque generated by the motor, and it will induce the lateral motion. We can imagine that the trajectory must be spiral since the vehicle is lifting up and turning clockwise.

These cases demonstrate the creditability of the dynamic model of MAVs. According to the above simulations and records from flight tests, we successfully obtain different trajectories that also occurs in flight test.

## IV. Conclusions

In this paper we study the dynamics of flapping-wing MAVs. Our results are also compared with the flight test data, using the flapping-wing MAVs developed by TKU MEMS Lab. Starting from Newton's second law, we derive the equations of motion for the MAVs. By observing the cruise flight of our MAVs in the high speed CCD Camera, we show that flapping doesn't affect the vertical motion of the whole vehicle, implying that the averaging theory is applicable. We also analytically prove that the time-average forces (lift and thrust) have the same formulation as those in the conventional fixed wing, while the only difference is the coefficient of lift, which is a function of advance ratio and set angle instead of angle of attack. As a result, having the force coefficient curves from wind tunnel test data, we can simulate the dynamics immediately without assuming the time history of those aerodynamics forces. Numerical simulations are also provided in this paper. Our numerical simulations not only catch the trend of the flight test trajectory, but also match the cruise flight condition.

## V. Acknowledgement

The work described here is funded by the National Science Council through project NSC 97-2221-E-032-017. The authors wish to thank Dr. Lung-Jieh Yang and his research group for providing flight test and wind tunnel test data.

## References

[1] M.H. Dickinson, F.O. Lehmann, and S.P. Sane, "Wing rotation and the aerodynamic basis of insect flight," *Science*, Vol. 284, pp. 1954-1960, 1999

[2] C. K. Hsu, *The Preliminary Design, Fabrication, and Testing of Flapping Micro Aerial Vehicles*, Ph.D. Dissertation, Tamkang University, 2008

[3] Z.A. Khan, and S.K. Agrawal, "Control of Longitudinal Flight Dynamics of a Flapping-Wing Micro Air Vehicle Using Time-Averaged Model and Differential Flatness Based Controller," *Proceedings of the 2007 American Control Conference*, pp. 5284-5289, 2007

[4] Dae-Kwan Kim, and Jae-Hung Han, "Smart flapping wing using Macro-Fiber Composite actuators," Proceeding of Smart Structures and Materials, 2006

[5] U.M. Norberg, *Vertebrate Flight: Mechanics, Physiology, Morphology, Ecology and Evolution*, Springer-Verlag, 1990

[6] W.F. Phillips, *Mechanics of Flight*, John Wiley & Sons, 2004

[7] T. Rakotomamonjy, M. Ouladsine, and T. Le Moing, "Modelization and Kinematics Optimization for a Flapping-Wing Microair Vehicle," *Journal of Aircraft*, Vol. 44, 2007

[8] L. Schenato, D. Campolo, and S. Sastry, "Controllability issuse in flapping flight for biomimic MAVs," *Proceedings of the 42nd IEEE Conference on Decision and Control*, pp. 6441-6447, 2003

[9] M. Sun, J. Wang and Y. Xiong, "Dynamic flight stability of hovering insects," *Acta Mechanica Sinica*, 2007

[10] J. Yan, R.J. Wood, S.S. Avadhanula, , R.S.M. Fearing, "Towards flapping wing control for a micromechanical flying insect," *IEEE International Conference on Robotics and Automation*, 2001

[11] Yang Lung-Jieh, Hsu Cheng-Kuei, Hsiao Fu-Yuen and Shen Yung-Kang, "A Micro-Aerial-Vehicle(MAV) with Figure-of-Eight Flapping Induced by Flexible Wing Frames" *47th AIAA Aerospace Sciences Meeting*, 2009, Orlando, Florida

[12] L.J. Yang, M.W. Kao, C.K. Hsu, C.W. Liao, I-C. Huang and P.T. Fang, "A biomimetic figure-of-eight flapping of micro aerial vehicles(MAVS) illuminated by LEDS," *Asia-Pacific Conference on Transducers and Micro/Nanotechnology (APCOT 2008)*, 2008, Tainan, Taiwan